Scientia Iranica F (2022) 29(6), 3570–3581

Sharif University of Technology
Scientia Iranica
Transactions F: Nanotechnology
http://scientiairanica.sharif.edu

Effect of MHD on Casson fluid with Arrhenius activation energy and variable properties

S.M. Atif*, **S. Shah**, **and A. Kamran**

Department of Mathematics, Capital University of Science and Technology, 44000, Islamabad,Pakistan.

Received 8 March 2021; received in revised form 13 July 2021; accepted 6 September 2021

KEYWORDS
Exponential variable viscosity;
Viscous dissipation;
Temperature thermal conductivity;
Arrhenius activation energy.

Abstract. The present study investigates MHD Casson nanofluid under the influence of exponential temperature-dependent thermal conductivity and variable viscosity past a stretching surface. After the application of similarity transformations, the governing partial differential equations of the modelled problem are converted into ordinary differential equations and then a solution is achieved with the assistance of the shooting method. The solution obtained with the help of shooting technique is used to analyze the distribution of mass and heat flux over sheet. The effects of various governing parameters on the dimensionless velocity, temperature, and concentration distribution were analyzed and discussed in detail. The simulations of the presented model demonstrated that the surface drag increases as each of the Casson parameter and temperature-dependent thermal conductivity parameter is boosted while the rate of heat transfer is diminished. It is also observed that an increment in the temperature near the surface is noted against the thermal conductivity parameter, whereas the opposite trend is observed away from the surface.

1. Introduction

When added to the conventional heat transfer fluids, nanoparticles give the underlying idea of heat enhancement agents called nanofluid. The ongoing research on heat transfer improvement in thermal transport processes cannot be conceived without nanofluids, given their numerical applications in science and technology. The development of the field can be found in a number of researches available on the topic of nanofluid. The scope of these studies ranges from experimental to numerical simulations based on mathematical models. Ying et al. [1] numerically handled the Al_2O_3-water nanofluid by considering both single- and two-phased nanofluid models in convectively heated tubes. The numerical results in their study deviated from the experiment at the maximum rate of 20%. Azam et al. [2] introduced the nanofluid into light with temperature-dependent thermal conductivity and heat source/sink. They observed that depression of the unsteadiness parameter led to an increase in Sherwood number. Das et al. [3] numerically evaluated the thermal performance of CuO nanofluids channel flow. A rise of 23% in the heat transfer rate was reported in their study when using nanofluid instead of conventional fluids. Juosh et al. [4] studied MHD viscoelastic nanofluid and reported dual solution of stagnation point past a porous stretching surface with radiation effect. He found that the acclivity in the Deborah number contributed to the upsurge of the drag coefficient. Rasheed et al. [5] analyzed MHD stagnation point in a nanofluid flow with a nonuniform thermal reservoir. Pal and Mandal [6] discussed magnetohydrodynamic stagnation point flow with suction effect and reported that the Sherwood number declined as the Lewis number increased. Abbasi et al. [7] highlighted the bioconvective stagnation point in Maxwell

*. *Corresponding author.*
E-mail address: dmt161001@cust.pk (S.M. Atif)

doi: 10.24200/sci.2021.57873.5452

nanofluid flow past a convectively heated surface. They observed that the energy, concentration, and density profiles of non-convective surfaces were higher than those of convectively heated surfaces. Lund et al. [8] carried out the stability analysis and reported the dual solution of MHD stagnation point Casson fluid. Their main observation was that the sign of the smallest eigenvalue was indicative of the stability of the first solution. Sheikholeslami et al. [9] analyzed the entropy and thermal behavior of nanomaterial through solar collector involving new tapes and concluded that the energy losses could be reduced using nanofluids and twisted tapes. For more details of nanofluid see [10–17].

Casson fluid is widely applied where the fluid exhibits non-Newtonian behavior with a threshold shear stress. This model is also employed in the field of medical science like blood flow behavior [18]. In addition, it describes the behavior of base fluids that are used as coolants in the food industry such as sodium alginate [19], xanthan gum [20], etc. Owing to its applications, it has been extensively analyzed by many researches on heat transfer. For instance, Hamid [21] examined the Ohmic dissipation effects in a Casson fluid flowing across a vertically erected needle. He also discussed the dual solutions obtained as a function of needle thickness and remarked that the Nusselt number and frictional effects increased with an increase in the needle thickness. Naqvi et al. [22] investigated the flow around a porous stretching cylinder of a Casson nanofluid. They concluded that an upsurge in the magnetic field intensity and dynamic plastic parameter retarded the flow while the thermal profile of these parameters was enhanced. Kamran et al. [23] offered Keller box solution of a Casson nanofluid over a horizontally elongating sheet slippery in nature and heated convectively. In the present study, the Casson parameter deteriorated the velocity of the fluid and enhanced the temperature.

Magnetohydrodynamics is widely applied to different issues in science and technology on an industrial scale, and the need for it is ever growing, especially in petroleum industry and metallurgical processes [24]. In such cases, the qualitative nature of the products depends on the rate at which the cooling takes place. Since its advent, it has been used in many studies to investigate its impact on the properties of the fluids. Numerous studies on the impact of MHD on the heat transfer rate can be found in the literature. For instance, Hsiao [25] studied the electrical magnetohydrodynamic Maxwell nanofluid with thermal radiation and viscous dissipation effects. Naz et al. [26] investigated the dynamics of hydromagnetic cross nanofluid in the presence of gyrotactic microorganisms. They employed the homotopy analysis method to determine a solution to the boundary layer equations. In another study, Atif et al. [27] looked at the magnetic aspect of tangent hyperbolic nanofluid past a stretching wedge. One of their key results was the rising behavior of the thermal profile with an increase in the Brownian motion, generalized Biot number, and thermophoresis parameter. Recently, Sheikholeslami et al. [28] conducted a study on flat plate solar collectors and photovoltaic systems in the presence of nanofluid. Using slip conditions, Shah et al. [29] studied the MHD Maxwell nanofluid considering the radiation and chemical reaction effects. According to the findings, the skin friction coefficient increased as the Maxwell parameter increased. Further information can be found in [30–35].

The concept of Arrhenius activation energy is the minimum chemical energy that molecules of a substance require to start a chemical reaction. This quantity of activation energy varies for different chemical substances. An early study of Arhenious energy was carried out by Bestman [36]. Recently, Nisar et al. [37] examined role of Arrhenius energy in peristaltic flow of Eyring-Powell nanofluid, considering the effect of thermal radiation. The results revealed that the concentration of the nanoparticles in the channel remained intact upon increasing the activation energy parameter. Another study was conducted by Azam et al. [38] who investigated the radiative cross nanofluid axisymmetric flow that developed covalent bonds and evaluated the impact of activation on that bonding. They came up with an interesting result, i.e., the concentration of nanoparticles increased with the elevation of activation energy values. Reddy et al. [39] employed RK-4th order technique to determine the solution of 3D-MHD Eyring Powell nanofluid flow over a slandering sheet with velocity and thermal slips.

To the best of authors' knowledge, no study has been conducted on the Casson nanofluid with temperature-dependent thermal conductivity, exponential viscosity, and Arrhenius activation energy yet. This study puts its main focus on four aspects: (a) addressing the heat and mass transfer of Casson nanofluid; (b) examining the impact of Joule heating and viscous dissipation effect; (c) analyzing the effect of exponential temperature-dependent thermal conductivity and variable viscosity on flow and thermal fields; and (d) performing the analysis of the convective heating boundary condition. The system of the resulting ODEs of the modeled problem is solved through shooting technique. Further, the prominent parameters affecting dimensionless quantities such as velocity, concentration, and temperature are graphically represented and investigated in detail.

2. Formulation of problem

A 2D viscous tangent hyperbolic forces the use of a sheet elongating at a rate of $u = ax$ in the x-

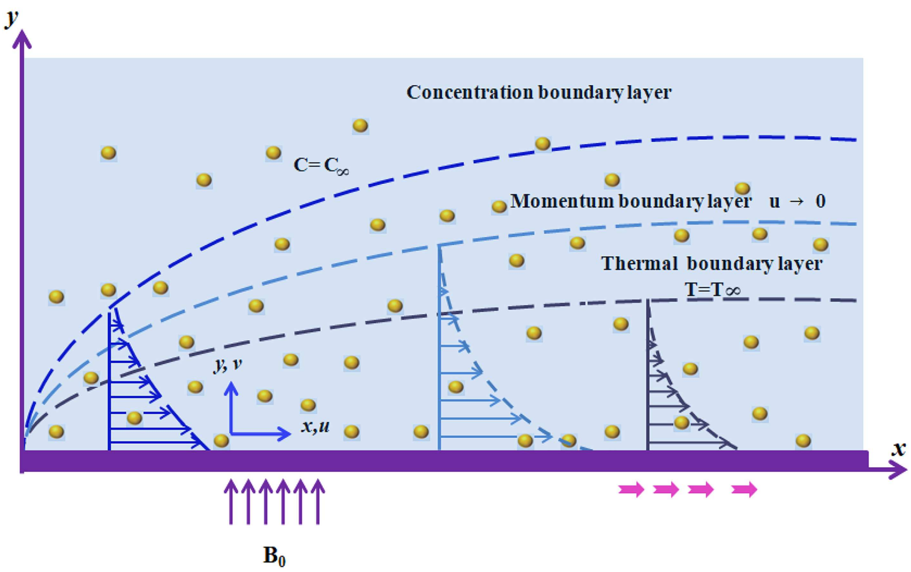

Figure 1. Geometrical setup of the problem.

direction. The fluid viscosity and thermal conductivity are assumed temperature dependent. Both temperature and velocity gradients are generated along the y-direction. Fluid is subjected to a temperature gradient on the surface far away from the sheet which is assumed to be at the constant temperature T_∞. The nanomaterial concentration on the surface far away from the walls and on the surface are regarded as C_∞ and C_w respectively. Magnetohydrodynamic impact is evaluated by considering a magnetic field of strength B_0 in the y-direction with significant Joule heating. The geometrical setup is demonstrated in Figure 1.

Contained in the above constraints, the governing equations of the problem above modeled are as follows:

$$\frac{\partial u}{\partial x}+\frac{\partial v}{\partial y}=0, \tag{1}$$

$$u\frac{\partial u}{\partial x}+v\frac{\partial u}{\partial y}=\frac{1}{\rho}\left(1+\frac{1}{\beta}\right)\left(\mu_\beta\frac{\partial u}{\partial y}\right)-\frac{\sigma B_0^2}{\rho}u, \tag{2}$$

$$u\frac{\partial T}{\partial x}+v\frac{\partial T}{\partial y}=\frac{1}{\rho C_p}\frac{\partial}{\partial y}\left(K(T)\frac{\partial T}{\partial y}\right)+\left(1+\frac{1}{\beta}\right)\frac{\mu_\beta}{\rho C_p}\left(\frac{\partial u}{\partial y}\right)^2+\frac{\sigma B_0^2}{\rho C_p}u^2+\frac{(\rho C_p)_p}{(\rho C_p)_f}\left[D_B\frac{\partial C}{\partial y}\frac{\partial T}{\partial y}+\frac{D_T}{T_\infty}\left(\frac{\partial T}{\partial y}\right)^2\right], \tag{3}$$

$$u\frac{\partial C}{\partial x}+v\frac{\partial C}{\partial y}=D_B\frac{\partial^2 C}{\partial y^2}+\frac{D_T}{T_\infty}\frac{\partial^2 T}{\partial y^2}-K_r^2\left(\frac{T}{T_\infty}\right)^m(C-C_\infty)e^{\left[\frac{-E_a}{KT}\right]}. \tag{4}$$

The associated BCs are:

$$u=u_w,\quad v=0,\quad -k\frac{\partial T}{\partial y}=h_f\,(T_f-T),$$

$$C=C_w\quad \text{at}\quad y=0,$$

$$u\to 0,\quad T\to T_\infty,\quad C\to C_\infty\quad \text{as}\quad y\to\infty. \tag{5}$$

Both thermal conductivity and dynamic viscosity of the fluid are assumed to be the exponential functions of the temperature difference calculated as follows:

$$\mu_\beta(T)=\mu_\beta^*\,e^{-\alpha^*\,(T-T_\infty)},$$

$$K(T)=K^*e^{-b(T-T_\infty)}.$$

In the temperature range of 0-400 F, the thermal conductivity changes linearly, thus we have:

$$K(T)\approx K^*(1-b(T-T_\infty)),$$

where, α^* is the variable viscosity, ϵ thermal conductivity parameters, μ_β^* and K^* denote constant coefficients of viscosity and thermal conductivity away from surface; b and α^* are the empirical constants that can take positive and negative value [40].

A set of transformations that leads to the non-dimensionalization of the governing equations is given as follows:

$$\eta=y\sqrt{\frac{a}{\nu}},\qquad \psi=x\sqrt{a\nu}f(\eta),$$

$$\theta(\eta)=\frac{T-T_\infty}{T_f-T_\infty},\qquad \phi(\eta)=\frac{C-C_\infty}{C_w-C_\infty}. \tag{6}$$

While using these transformations, Eq. (1) is satisfied identically and Eqs. (2)-(4) are reduced to:

$$\left(1+\frac{1}{\beta}\right)e^{-\gamma\theta}\left(f'''-\gamma f''\theta'\right)-f'^2-Mf'+ff''=0, \tag{7}$$

$$(1-\epsilon\theta)\theta'' + Pr\left[\left(1+\frac{1}{\beta}\right) Ec\, e^{-\gamma\theta} f''^2 + f\theta' + Nb\theta'\phi' + Nt\theta'^2 + EcMf'^2\right] - \epsilon\theta'^2 = 0, \quad (8)$$

$$\phi'' + Sc\, f\phi' - Sc\, \delta\phi(1+\theta(\theta_w - 1))^m e^{\left(\frac{E}{1+\theta(\theta_w-1)}\right)} + \frac{Nt}{Nb}\theta''. \quad (9)$$

The transformed BCs are:

$$f(\eta)=0, \quad f'(\eta)=1, \quad \theta'(\eta) = \frac{-Bi}{1-\epsilon\theta(\eta)}(1-\theta(\eta)),$$

$$\phi(\eta)=1, \quad \text{at} \quad \eta=0,$$

$$f' \to 0, \quad \theta \to 0, \quad \phi \to 0, \qquad \text{as} \qquad \eta \to \infty. \quad (10)$$

In the above equations $\gamma = -\alpha^*(T_f - T_\infty)$ represents the temperature-dependent viscosity parameter, $Bi = \frac{h}{k}\sqrt{\frac{\nu}{a}}$ the Biot number, $Nb = \frac{\Lambda D_B(C_w - C_\infty)}{\nu}$ the Brownian motion parameter, $Sc = \frac{\nu}{D_B}$ the Schmidt number, $Ec = \frac{a^2x^2}{(C_p)_f(T_f - T_\infty)}$ the Eckert number, $M = \frac{\sigma B_0^2}{a\rho}$ the magnetic number, $Pr = \frac{\nu}{\alpha}$ the Prandtl number, $\epsilon = b(T_f - T_\infty)$ the thermal conductivity parameter, $Nt = \frac{\Lambda D_T(T_f - T_\infty)}{\nu T_\infty}$ the thermophoresis parameter, $\theta_w = \frac{T_f}{T_\infty}$ the temperature ratio parameter, $E = \frac{E_a}{KT_\infty}$ the Arrhenius activation energy, and $\delta = \frac{k_r^2}{b}$ the rate of chemical reaction.

3. Physical quantities

The physical quantities such as surface drag C_f, temperature gradient Nu, and concentration gradient Sh on the surface are given as follows:

$$C_f = \frac{\tau_w}{\rho_f u_w^2}, \qquad Nu = \frac{xq_w}{k(T_f - T_\infty)}$$

$$Sh = \frac{xj_w}{k(T_f - T_\infty)}.$$

In the non-dimensional form, we have:

$$C_f Re_x^{1/2} = (1-\epsilon\theta)\left(1+\frac{1}{\beta}\right) f''(0),$$

$$Nu_x Re_x^{-1/2} = -(1-\epsilon\theta(0))\theta'(0),$$

$$Sh_x Re_x^{-1/2} = -\phi'(0), \quad (11)$$

where $Re_x = \frac{ax^2}{\nu}$ represents local Reynolds number.

4. Implementation of the method

The solution of the below system of Eqs. (12) subject to BCs is achieved using shooting technique [41] along with the fourth-order Runge Kutta method. A suitable domain $[0, \eta_{\max}]$ instead of $[0, \infty)$ was taken into consideration for the simulations such that there will be no fluctuations in the computed results. The criteria for stopping the iterative process are set as follows:

$$\max\{|\chi_2(\eta_{\max}) - 0|, |\chi_4(\eta_{\max}) - 0|, |\chi_6(\eta_{\max}) - 0|\} < 10^{-6}.$$

The following new variables are introduced: $\chi_1 = f$, $\chi_2 = f'$, $\chi_3 = f''$, $\chi_4 = \theta$, $\chi_5 = \theta'$, $\chi_6 = \phi$, and $\chi_7 = \phi'$. Eqs. (7)-(9) were transformed into the following system of the first-order ordinary differential equations:

$$\chi_1' = \chi_2,$$

$$\chi_2' = \chi_3,$$

$$\chi_3' = \frac{1}{1+\frac{1}{\beta}}\left[\chi_2^2 - \chi_1\chi_3 + M\chi_2\right] e^{\gamma\chi_4} + \gamma\, \chi_3\chi_5,$$

$$\chi_4' = \chi_5,$$

$$\chi_5' = \frac{1}{1-\epsilon\,\chi_4} \left[-Pr(\chi_1\chi_5 + Nb\chi_5\chi_7 + Nt\,\chi_5^2 + \left(1+\frac{1}{\beta}\right) Ec\, e^{\gamma\chi_4} + Ec\chi_3^2) + \epsilon\chi_5^2\right],$$

$$\chi_6' = \chi_7,$$

$$\chi_7' = -Sc\chi_1\chi_7 + Sc\delta\chi_6(1+\chi_4(\theta_w+1))^m e^{\frac{E}{1+\chi_4(\theta_w+1)}} - (\frac{Nt}{Nb})\chi_5', \quad (12)$$

with boundary conditions:

$$\chi_1(\eta)=0, \quad \chi_2(\eta)=1,$$

$$\chi_5(\eta) = \frac{Bi}{1-\epsilon\theta(\eta)}(\chi_4(\eta)-1),$$

$$\chi_6(\eta)=1 \quad \text{at} \quad \eta=0,$$

$$\chi_2 \to 0, \quad \chi_4 \to 0, \quad \chi_6 \to 0, \quad \text{as} \quad \eta \to \infty. \quad (13)$$

5. Code validation

For verification of the correctness of the code, the results from the Skin friction coefficient which were obtained by Nadeem et al. [42], Ahmad and Nazar [43], and Ullah et al. [44] were successfully reproduced. Our simulations are in excellent agreement with the already published results obtained by Nadeem et al. [42],

Table 1. Comparison between the present values of $C_f Re_x^{1/2}$ with the already published values when $m = E = \theta_w = Sc = \delta = \gamma = \epsilon = Nt = Nb = Ec = 0$ and $Pr = 6.8, Bi \to \infty$.

M	β	[42]	[43]	[44]	Present results
0	∞	1.0042	1.0042	1	1.000008
	5	1.0954		1.0955	1.095584
	1	1.4142		1.4144	1.414441
10	∞	3.3165	3.3165	3.3166	3.316625
	5	3.6331		3.6332	3.633180
	1	4.6904		4.6904	4.690416
100	∞	10.049	10.0498	10.0499	10.049876
	5	11.0091		11.0091	11.009087
	1	14.2127		14.2127	14.212670

Ahmad and Nazar [43], and Ullah et al. [44] in the literature, as presented in Table 1.

6. Results and discussion

Table 2 presents evaluation of the effect of the pertinent parameters on the skin friction coefficient $C_f Re_x^{1/2}$. According to the growing values for each of the magnetic parameters M and γ, the temperature-dependent viscosity parameter causes increase in the skin friction coefficient, whereas it is reduced as the Casson parameter β is boosted. According to Table 3, an increase in each magnetic number M, temperature-dependent viscosity parameter γ, thermal conductivity parameter, ϵ, the Prandtl number Pr, Eckert number Ec, Brownian motion parameter, and thermophoresis parameter Nt would increase the Nusselt number $Nu_x Re_x^{-1/2}$, however it increases upon increasing Biot number Bi.

Figures 2–21 provide a better observation of the effect of the behavior of the physical parameters appearing in Eqs. (1)–(3), caused by a conversion from dimensional PDEs to non-dimensional ODEs, on the velocity f', temperature $\theta(\eta)$, and concentration $\phi(\eta)$ distribution. The velocity profile against the Casson fluid parameter β is presented in Figure 2. Accordingly, when β gets higher values, the velocity filed is reduced. This can be physically expected because the plastic

Table 2. Numerical values of $C_f Re_x^{1/2}$ when $m = 1, Pr = 7, \theta_w = 1.5, Sc = 1.2, \epsilon = 0.3, Nt = \delta = Nb = 0.1, Bi = 0.2, Ec = 0.02$ and $E = 0.1$.

M	β	γ	$C_f Re_x^{1/2}$
3	0.2	0.1	4.551534
4			5.027880
5			5.443501
	0.6		3.054347
	0.8		2.808729
	10		1.970544
	∞		1.879330
		0.2	4.651524
		0.3	4.753358
		0.4	4.857050

Table 3. Numerical values of $Nu_x Re_x^{-1/2}$ when $m = 1$, $\theta_w = 1.5$, $Sc = 1.2$, $\beta = 0.2$, $\delta = 0.1$ and $E = 0.1$.

M	γ	ϵ	Pr	Ec	Bi	Nb	Nt	$Nu_x Re_x^{-1/2}$
3	0.1	0.3	7.0	0.02	0.2	0.1	0.1	0.139346
4								0.130543
5								0.122144
	0.2							0.139333
	0.3							0.139322
	0.4							0.139311
		0.0						0.140795
		0.1						0.140336
		0.2						0.139854
			7.0					0.139346
			10					0.136769
			100					0.037747
				0.01				0.158642
				0.02				0.139346
				0.03				0.119525
					0.2			0.139346
					0.4			0.247300
					0.6			0.332236
						0.2		0.129837
						0.3		0.117658
						0.4		0.101811
							0.2	0.137535
							0.3	0.135523
							0.4	0.133264

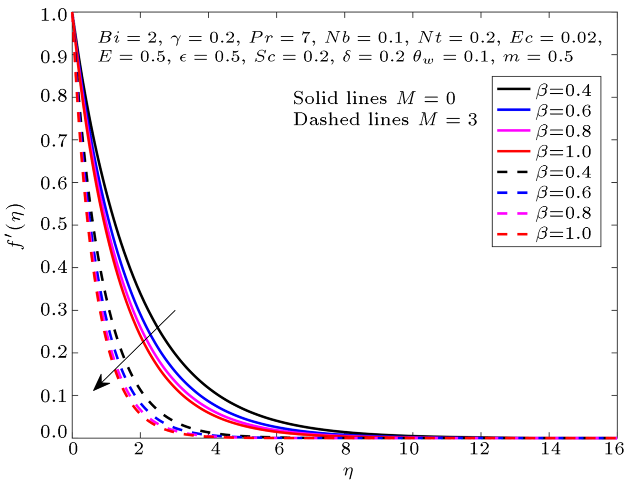

Figure 2. Variation in f' due to β.

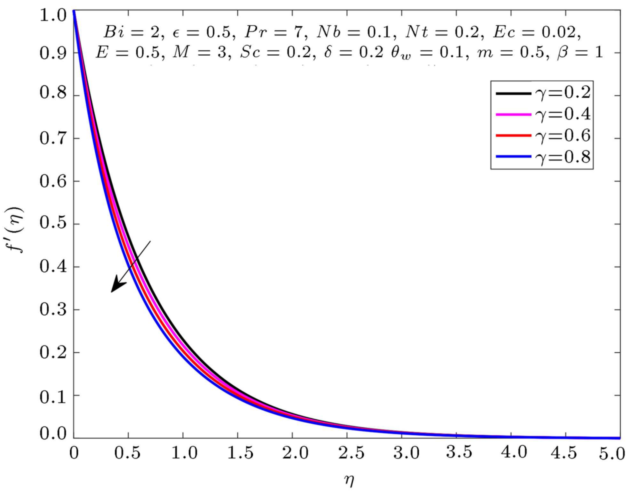

Figure 3. Variation in f' due to γ.

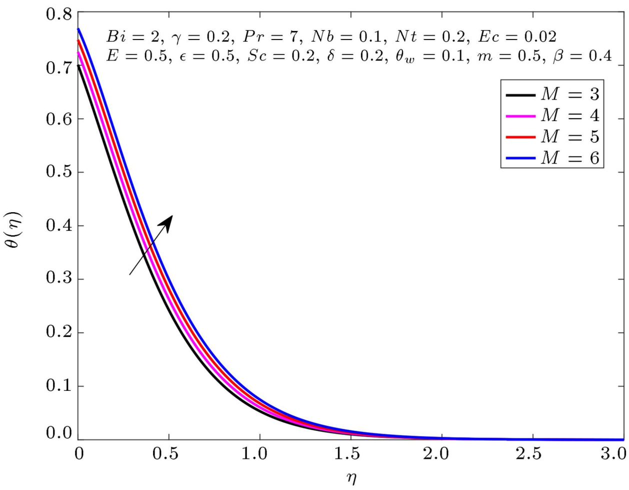

Figure 4. Variation in θ due to M.

dynamic viscosity of the fluid increases upon increasing β. This increase in return leads to the formation of resistivity in the flow of fluid, which causes a decrease in the fluid velocity. As observed in the same figure, a reduction in the velocity is more prominent under the impact of the magnetic field. Magnetic effects cause resistance in the fluid flow due to which the velocity is significantly subsided in the presence of magnetic effects. Figure 3 evaluates the impact of viscosity parameter γ on the non-dimensional $f'(\eta)$. According to this figure, $f'(\eta)$ is boosted with a reduction in the viscosity parameter. Physically, the higher the viscosity parameter γ is, the thicker the particles of the fluid will be, thus leading to a decrease in the velocity.

Figures 4–9 show the variations in temperature distribution against the values of the sundry parameters. According to Figure 4, the temperature increases at higher magnetic parametric values. The impact of the Prandtl number Pr on the temperature is given in Figure 5 where a decreasing trend is observed, as expected. Figure 6 evaluates the impact of parameter Nb, the Brownian motion parameter, on the temperature field. The temperature needed for increasing the parametric values of Nb increases mainly due to the abrupt rapid random motion of the species particles present in nanofluid. The Brownian forces resulting from the increasing random motion of particles increase, which enhanced heat transportation. Figure 7 illustrates the effect of thermophoresis on the temperature field. Following the increasing values of Nt, the thermophoretic parameter which is the fluid temperature increases. The nanoparticles move from a hotter region to a cooler one because of thermophoretic force, hence more heat transfers in the region of boundary layer. The effect of viscous dissipation is described by Eckert number Ec. The Eckert number, Ec, represents the relation between the kinetic energy and change in enthalpy. Figure 8 is outlined to visualize the effect of Ec on energy profile. An increase in Ec causes an acclivity in the thermal profile. Physically, upon increasing the dissipation, the thermal conductivity is enhanced, thus increasing the temperature profile. The temperature

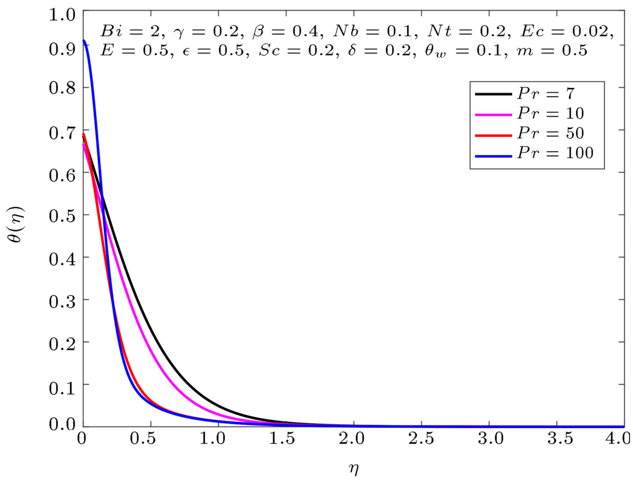

Figure 5. Variation in θ due to Pr.

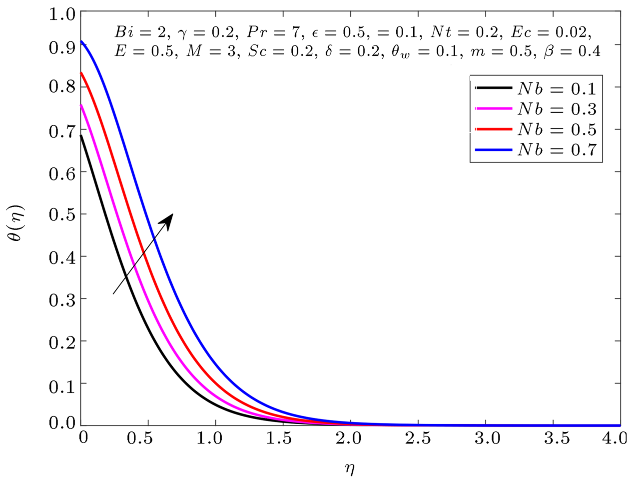

Figure 6. Variation in θ due to Nb.

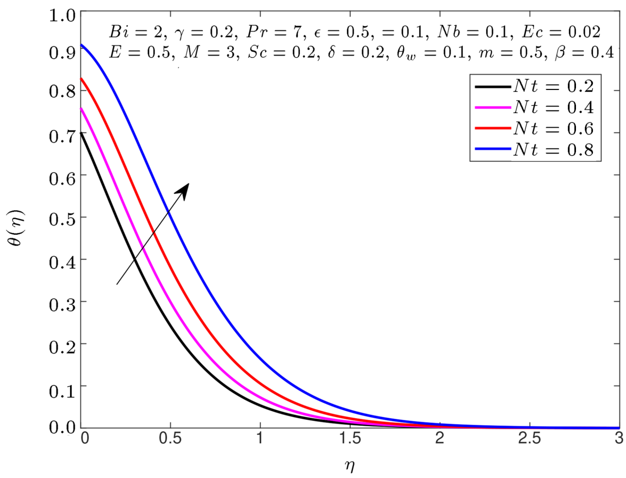

Figure 7. Variation in θ due to Nt.

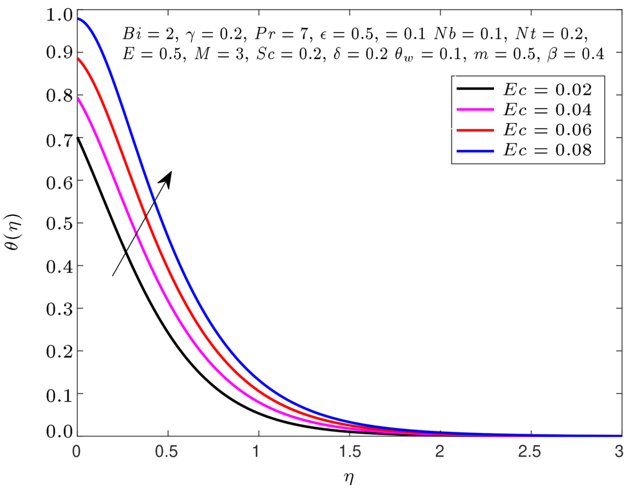

Figure 8. Variation in θ due to Ec.

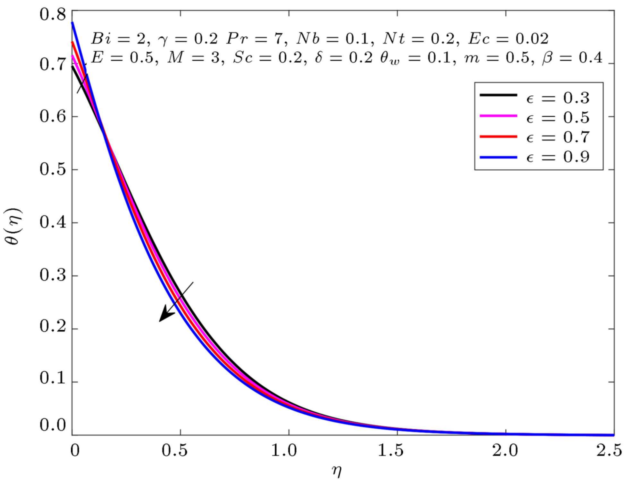

Figure 9. Variation in θ due to ϵ.

against the variable thermal conductivity parameter is examined and presented in Figure 9. An increase in the temperature distribution near the boundary is observed and it decreases away from the surface.

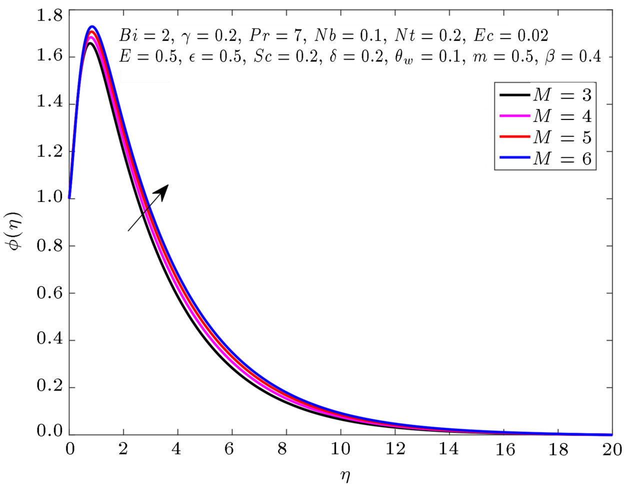

Figure 10. Variation in ϕ due to M.

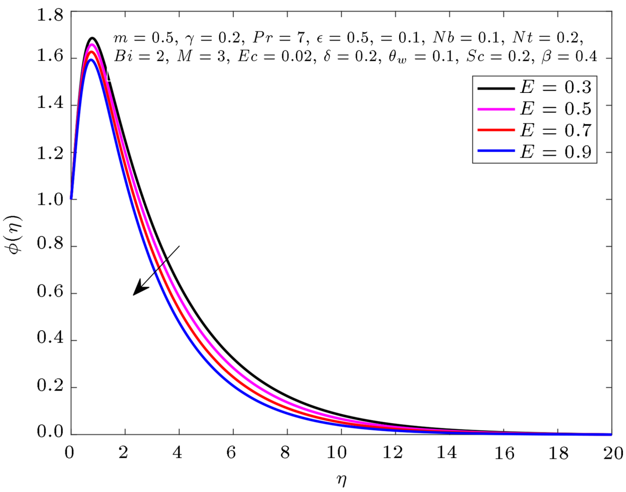

Figure 11. Variation in ϕ due to E.

Figure 10 evaluates the effect of the magnetic parameter M on the concentration profile ϕ. As observed, ϕ follows a decreasing trend at larger values of M. The effect of E on ϕ is shown in Figure 11. Following an increase in the value of E, ϕ is reduced. Figures 12 and 13 show the effect of Nb and Nt on $\phi(\eta)$. As observed, the concentration profile $\phi(\eta)$ increases at higher values of Brownian motion parameter Nb. An increase in the Brownian motion leads to an increase in the motion of the small particles inside the flow region. This enhanced chaotic movement intensifies the velocity of the particles that in turn causes an increase in the kinetic energy and the depreciation of the concentration field is observed, which is evident from the figure, whereas an opposite trend in concentration profile $\phi(\eta)$ is depicted for the growing values of Nt. Physically, in thermophoresis, the particles apply force on the other particles due to which particles from the hotter region move towards the colder region. Larger values of Nt imply the application of the force on the other particles and, as a result, more fluid moves

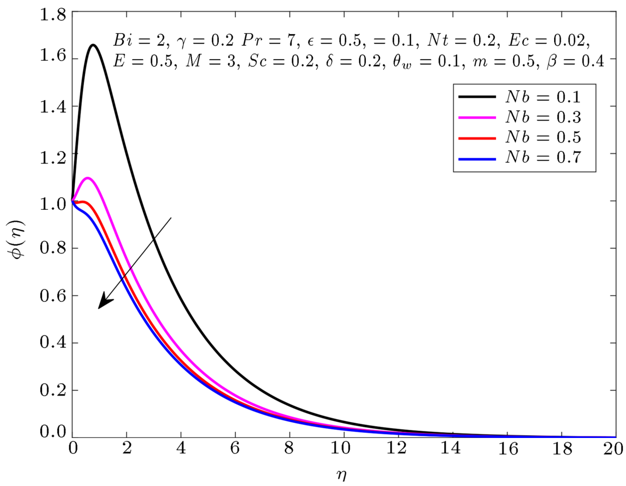

Figure 12. Variation in ϕ due to Nb.

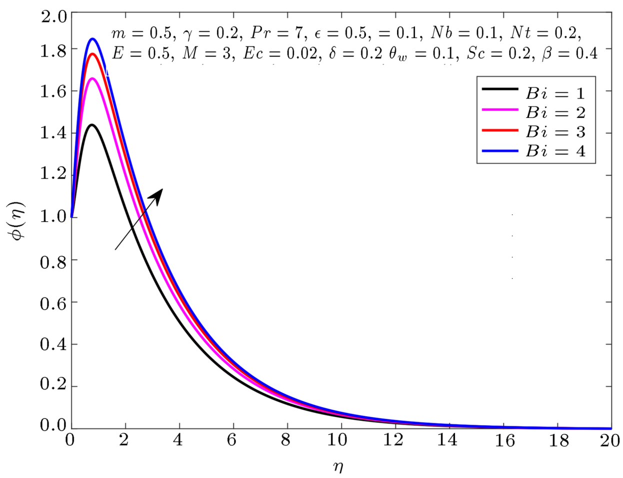

Figure 15. Variation in ϕ due to Bi.

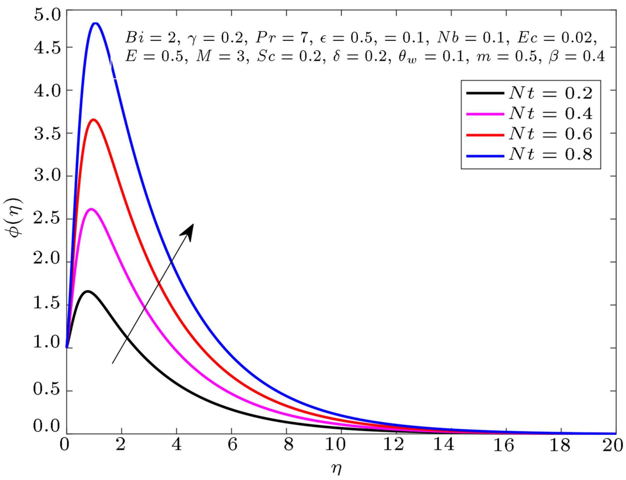

Figure 13. Variation in ϕ due to Nt.

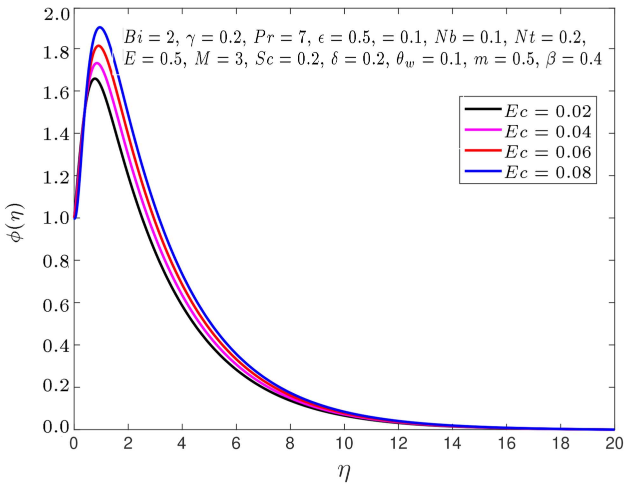

Figure 16. Variation in ϕ due to Ec.

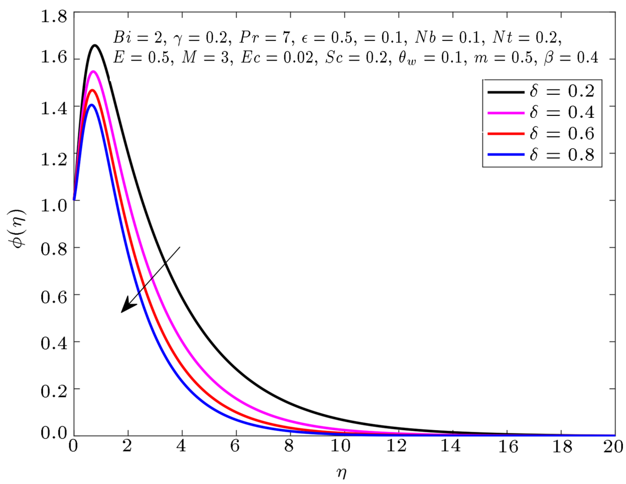

Figure 14. Variation in ϕ due to δ.

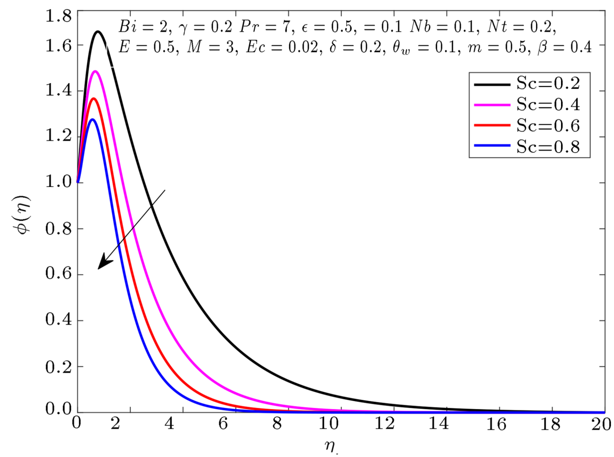

Figure 17. Variation in ϕ due to Sc.

from the higher-temperature region to a less hotter region. Therefore, this increment in the nanoparticle's concentration is noticed. The concentration profile ϕ against the values of δ is placed in Figure 14. A decline in $\phi(\eta)$ is noted when δ increases. An increase is also observed in ϕ when the values of Bi and Ec increase, as shown in Figures 15 and 16, whereas it decreases against the increasing values of Sc, as shown in Figure 17.

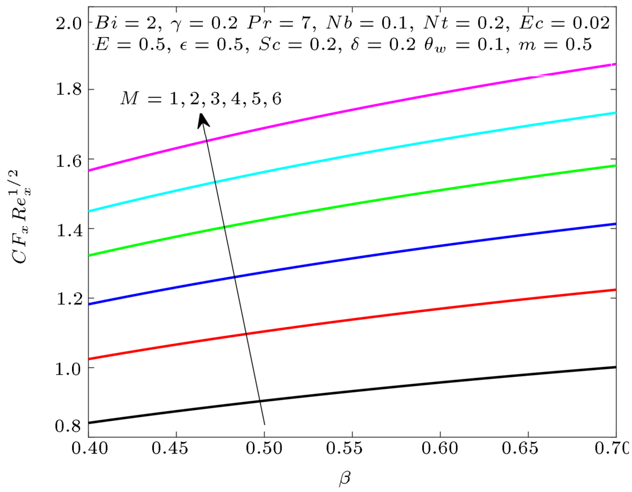

Figure 18. Effect of M and β on $Cf_x Re_x^{\frac{1}{2}}$.

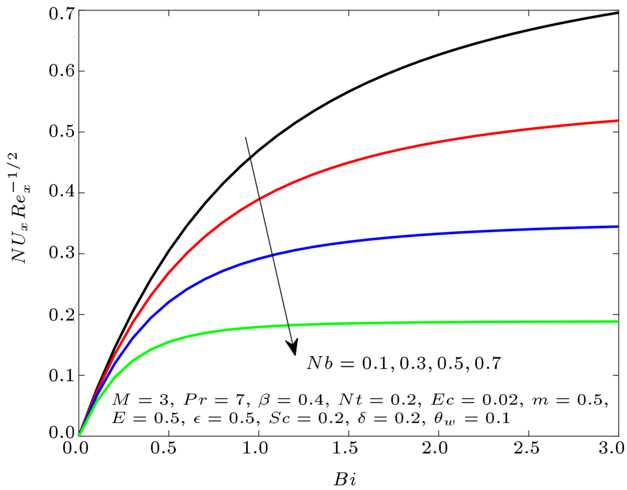

Figure 20. Effect of Nb and Bi on $Nu_x Re_x^{-\frac{1}{2}}$.

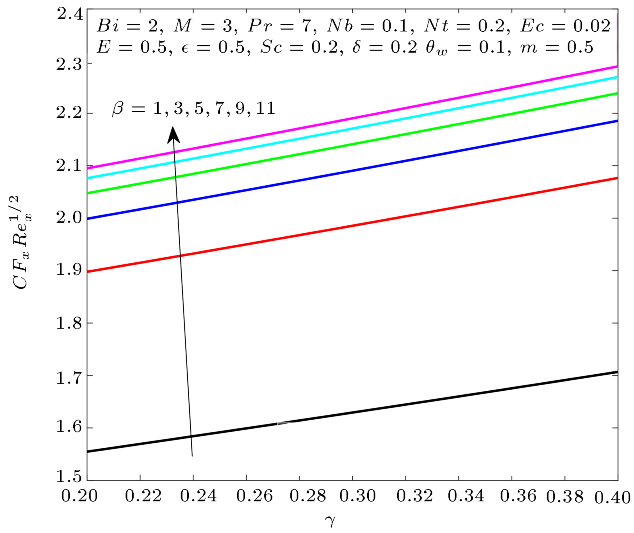

Figure 19. Effect of β and γ on $Cf_x Re_x^{\frac{1}{2}}$.

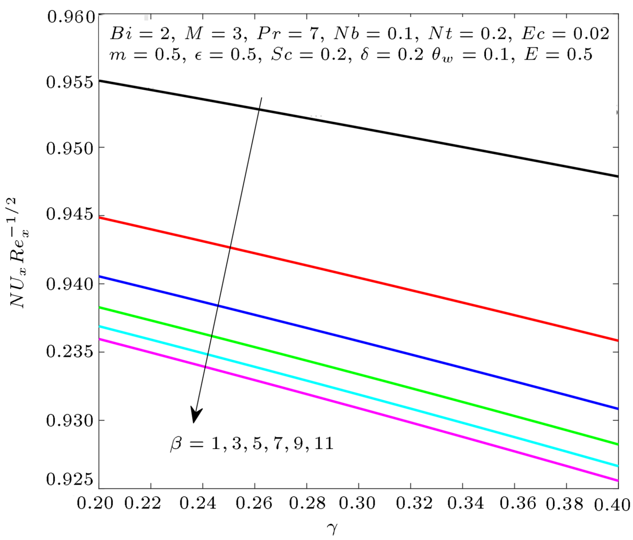

Figure 21. Effect of β and γ on $Nu_x Re_x^{-\frac{1}{2}}$.

The skin-friction coefficient $Cf_x Re_x^{1/2}$ against the values of M and β is given in Figure 18. According to this figure, $Cf_x Re_x^{1/2}$ is an increasing function of both the parameters M and β. In the next figure, the effect of γ along β on $Cf_x Re_x^{1/2}$ is shown. The similar behavior of $Cf_x Re_x^{1/2}$ is noted against γ along with β, as shown in Figure 19. The Nusselt number $Nu_x Re_x^{-1/2}$ against the values of Bi and Nb is presented in Figure 20, indicating that $Nu_x Re_x^{-1/2}$ is a decreasing function of both the parameters Bi and Nb. Figure 21 evaluates the effect of γ along β on $Nu_x Re_x^{-1/2}$. Similar behavior of $Nu_x Re_x^{-1/2}$ against γ along with β is also observed.

7. Final remarks

In the present study, prominent parameters effecting velocity, concentration, and temperature distributions are investigated in detail. Some of the key features are as follows:

- An increase in the temperature profile near the surface was observed upon increasing the thermal conductivity parameter; however, an opposite trend was observed far away from the surface;
- An augmentation in the Casson parameter β would decrease the velocity profile;
- The temperature distribution was diminished at the growing values of the Prandtl number Pr;
- The skin-friction $Cf_x\ Re_x^{1/2}$ was an increasing function of both Casson parameters β and γ whereas the Nusselt number $Nu_x Re_x^{-1/2}$ decreased for both β and γ;
- There was a decrease in the concentration distribution $\phi(\eta)$ upon increasing the Brownian motion

parameter Nb; however, thermophoresis parameter Nt exhibited opposite behavior.

Nomenclature

B_0	Applied magnetic field
C_∞	Ambient concentration
C	Boundary layer concentration
C_p	Specific heat
C_f	Skin friction coefficient
C_0	Initial reference concentration
C_w	Concentration at wall surface
D_T	Thermophoresis diffusion parameter
D_B	Brownian diffusion coefficient
E	Arrhenius activation energy
Ec	Eckert number
h_w	Local surface heat flux
k	Thermal conductivity
Lb	Bioconvection Lewis number
M	Magnetic number
Nu_x	Nusselt number
Nt	Thermophoresis parameter
Nb	Brownian motion parameter
Pr	Prandtl number
Rd	Thermal radiation parameter
q_r	Radiative heat flux
Sc	Schmidt number
T_0	Initial reference temperature
T	Boundary layer temperature
T_w	Surface temperature
T_∞	Ambient temperature
t	Time
u, v	Velocity components
u_w	Characteristics velocity
We	Weissenberg number

Greek letters

ν	Kinematic viscosity
ρ	Fluid density
μ	Dynamic viscosity
σ	Electric charge density
ϕ	Dimensionless concentration
δ	Rate of chemical reaction
γ	Temperature dependent viscosity parameter
θ	Dimensionless temperature
ϵ	Thermal conductivity parameter
$(\rho C_p)_f$	Heat capacity of the fluid
$(\rho C_p)_p$	Heat capacity of the nanoparticals
η	Dimensionless boundary layer thickness
β	Casson parameter

References

1. Ying, Z., He, B. He, D., et al. "Comparisons of single-phase and two-phase models for numerical predictions of Al2O3/water nanofluids convective heat transfer", *Advanced Powder Technology*, **31**(7), pp. 3050–3061 (2020).

2. Azam, M., Xu, T., and Khan, M. "Numerical simulation for variable thermal properties and heat source/sink in flow of Cross nanofluid over a moving cylinder", *International Communications in Heat and Mass Transfer*, **118**, p. 104832 (2020).

3. Das, R.K., Sokhal, G.S., and Sehgal, S.S. "A numerical study on the performance of water based copper oxide nanofluids in compact channel", *Materials Today: Proceedings* (2020).

4. Jusoh, R., Nazar, R., and Pop, I. "Dual solutions of magnetohydrodynamic stagnation point flow and heat transfer of viscoelastic nanofluid over a permeable stretching/shrinking sheet with thermal radiation", *Journal of Physics: Conference Series*, **890**(1), 012063 (2017).

5. Rasheed, H.U., Islam, S., Noor, S., et al. " Impact of magneto hydro dynamics on stagnation point slip flow due to nonlinearly propagating sheet with nonuniform thermal reservoir", *Mathematical Problems in Engineering*, **2020** (2020).

6. Pal, D. and Mandal, G. "Magnetohydrodynamic stagnation point flow of Sisko nanofluid over a stretching sheet with suction", *Propulsion and Power Research*, **9**(4), pp. 408–422 (2020).

7. Abbasi, A., Farooq, W., and Riaz, I. "Stagnation point flow of Maxwell nanofluid containing gyrotactic microorganism impinging obliquely on a convective surface", *Heat Transfer*, **49**(5), pp. 2977–2999. (2020).

8. Lund, L.A., Omar, Z., Khan, I., et al. "Dual similarity solutions of MHD stagnation point flow of Casson fluid with effect of thermal radiation and viscous dissipation: stability analysis", *Scientific Reports*, **10**(1), pp. 1–13 (2020).

9. Sheikholeslami, M., Farshad, S.A., and Said, Z. "Analyzing entropy and thermal behavior of nanomaterial through solar collector involving new tapes", *International Communications in Heat and Mass Transfer*, **123**, p. 105190 (2021).

10. Hsiao, K.L. "To promote radiation electrical MHD activation energy thermal extrusion manufacturing system efficiency by using Carreau nanofluid with parameters control method", *Energy*, **130**, pp. 486–499 (2017).

11. Hsiao, K.L. "Stagnation electrical MHD nanofluid mixed convection with slip boundary on a stretching sheet", *Applied Thermal Engineering*, **98**, pp. 850–861 (2016).

12. Chakraborty, S. and Panigrahi, P.K. "Stability of nanofluid: A review", *Applied Thermal Engineering*, p. 115259 (2020)

13. Khan, M.I., Hafeez, M.U., Hayat, T., et al. "Magneto rotating flow of hybrid nanofluid with entropy generation",*Computer Methods and Programs in Biomedicine*, **183**, p. 105093 (2020).

14. Izadi, A., Siavashi, M., Rasam, H., et al. "MHD enhanced nanofluid mediated heat transfer in porous metal for CPU cooling", *Applied Thermal Engineering*, **168**, p. 114843 (2020).

15. Atif, S.M., Hussain, S. and Sagheer, M. "MHD micropolar nanofluid with non Fourier and non Fick's law", *International Communications in Heat and Mass Transfer*, **122**, p. 105114 (2021).

16. Sheikholeslami, M. and Farshad, S.A. "Investigation of solar collector system with turbulator considering hybrid nanoparticles", *Renewable Energy*, **171**, pp. 1128–1158 (2021).

17. Atif, S.M., Hussain, S., and Sagheer, M. "Effect of thermal radiation on MHD micropolar Carreau nanofluid with viscous dissipation, Joule heating, and internal heating", *Scientia Iranica*, **26**(6), pp. 3875–3888 (2019).

18. Aneja, M., Chandra, A., and Sharma, S. "Natural convection in a partially heated porous cavity to Casson fluid", *International Communications in Heat and Mass Transfer*, **114**, p. 104555 (2020).

19. Alwawi, F.A., Alkasasbeh, H.T., Rashad, A.M., et al. "MHD natural convection of sodium alginate Casson nanofluid over a solid sphere", *Results in Physics*, **16**, pp. 102818 (2020).

20. Salehi, F. "Effect of common and new gums on the quality, physical, and textural properties of bakery products: A review", *Journal of Texture Studies*, **51**(2), pp. 361–370 (2020).

21. Hamid, A. "Terrific effects of Ohmic-viscous dissipation on Casson nanofluid flow over a vertical thin needle: buoyancy assisting & opposing flow", *Journal of Materials Research and Technology*, **9**(5), pp. 11220–11230 (2020).

22. Naqvi, S.M.R.S., Muhammad, T., and Asma, M. "Hydromagnetic flow of Casson nanofluid over a porous stretching cylinder with newtonian heat and mass conditions", *Physica A: Statistical Mechanics and Its Applications*, p. 123988 (2020).

23. Kamran, A., Hussain, S., Sagheer, M., et al. "A numerical study of magnetohydrodynamics flow in Casson nanofluid combined with Joule heating and slip boundary conditions", *Results in Physics*, **7**, pp. 3037–3048 (2017).

24. Ren, Z., Lei, Z., Li, C., et al. "New study and development on electromagnetic field technology in metallurgical processes", *Acta Metallurgica Sinica*, **56**(4), pp. 583–600, (2020).

25. Hsiao, K.L. "Combined electrical MHD heat transfer thermal extrusion system using Maxwell fluid with radiative and viscous dissipation effects", *Applied Thermal Engineering*, **112**, pp. 1281–1288 (2017).

26. Naz, R., Noor, M., Hayat, T., et al. "Dynamism of magnetohydrodynamic Cross nanofluid with particulars of entropy generation and gyrotactic motile microorganisms", *International Communications in Heat and Mass Transfer*, **110**, p. 104431 (2020).

27. Atif, S.M., Hussain, S., and Sagheer, M. "Heat and mass transfer analysis of time-dependent tangent hyperbolic nanofluid flow past a wedge," *Physics Letters A*, **283**(11), pp. 1187–1198 (2019).

28. Sheikholeslami, M., Farshad, S.A., Ebrahimpour, et al. "Recent progress on flat plate solar collectors and photovoltaic systems in the presence of nanofluid: A review", *Journal of Cleaner Production*, **293**, p. 126119 (2021).

29. Shah, S., Atif, S.M., and Kamran, A. "Radiation and slip effects on MHD Maxwell nanofluid flow over an inclined surface with chemical reaction", *Heat Transfer*, **50**(4), pp. 4062–4085 (2021).

30. Hsiao, K.L. "Micropolar nanofluid flow with MHD and viscous dissipation effects towards a stretching sheet with multimedia feature", *International Journal of Heat and Mass Transfer*, **112**, pp. 983–990, (2017).

31. Atif, S.M., Hussain, S., and Sagheer, M. "Effect of thermal radiation and variable thermal conductivity on magnetohydrodynamics squeezed flow of Carreau fluid over a sensor surface", *Journal of Nanofluid*, **8**, pp. 806–816 2019.

32. Akmal, N., Sagheer, M., Hussain, S., et al. "Study of micropolar nanofluids with power-law spin gradient viscosity model by the Keller box method", *Canadian Journal of Physics*, **8**(4), pp. 16–27 (2020).

33. Shah, S., Hussain, S., and Sagheer, M. "Thermal stratification effects on mixed convective Maxwell fluid flow with variable thermal conductivity and homogeneous/heterogeneous reactions", *Journal of the Brazilian Society of Mechanical Sciences and Engineering*, **40**, pp. 452–463 (2018).

34. Atif, S.M., Hussain, S., and Sagheer, M. "Effect of viscous dissipation and Joule heating on MHD radiative tangent hyperbolic nanofluid with convective and slip conditions", *Journal of the Brazilian Society of Mechanical Sciences and Engineering*, **41**(4), pp. 189–206 (2019).

35. Atif, S.M., Abbas, M., Rashid, U., et al. "Stagnation point flow of EMHD micropolar nanofluid with mixed convection and slip boundary", *Complexity*, **2021** (2021).

36. Bestman, A.R. "Natural convection boundary layer with suction and mass transfer in a porous medium",

International Journal of Energy Research, **14**(4), pp. 389–396 (1990).

37. Nisar, Z., Hayat, T., Alsaedi, A., et al. "Significance of activation energy in radiative peristaltic transport of Eyring Powell nanofluid", *International Communications in Heat and Mass Transfer*, **116**, p. 104655 (2020).

38. Azam, M., Xu, T., Shakoor, A., et al. "Effects of Arrhenius activation energy in development of covalent bonding in axisymmetric flow of radiative Cross nanofluid", *International Communications in Heat and Mass Transfer*, **113**, p. 104547 (2020).

39. Reddy, S.R.R., Reddy, P.B.A., and Bhattacharyya, K. "Effect of nonlinear thermal radiation on 3D magneto slip flow of Eyring-Powell nanofluid flow over a slendering sheet with binary chemical reaction and Arrhenius activation energy", *Advanced Powder Technology*, **30**(12), pp. 3203–3213 (2019).

40. Jangilis, S., Adesanya, S.O., and Ogunseye, H.A. "Couple stress fluid flow with variable properties: a second law analysis", *Mathematical Methods in Applied Science*, **42**, pp. 85–98 (2019).

41. Na, T.Y., *Computational Methods in Engineering Boundary Value Problems*, **145**, Academic Press (1979).

42. Nadeem, S., Haq, R.U., and Akbar, N.S. "MHD three dimensional boundary layer flow of Casson nanofluid past a linearly stretching sheet with convective boundary condition", *IEEE Transactions on Nanotechnology*, **13**(1), pp. 109–115 (2014).

43. Ahmad, K. and Nazar, R. "Magnetohydrodynamic three dimensional flow and heat transfer over a stretching surface in a viscoelastic fluid", *Journal of Science and Technology*, **3** (2011).

44. Ullah, I., Khan, I., and Shafie, S. "MHD natural convection flow of Casson nanofluid over nonlinearly stretching sheet through porous medium with chemical reaction and thermal radiation", *Nanoscale Research Letters*, **3**, pp. 527–539 (2016).

Biographies

Shahzada Muhammad Atif completed his PhD in Fluid Mechanics from Capital University of Science and Technology, Islamabad, Pakistan in 2020. Dr. Atif has more than 10 publications in reputable journals. He has more than 20 years of teaching experience. His research interests are fluid dynamics, magnetohydrodynamics, properties of nanofluids, and their heat transfer characteristics.

Sajid Shah is working as an Assistant Professor at the Department of Mathematics at Government Post Graduate College, Asghar Mall, Rawalpindi, Pakistan. He received his PhD in Fluid Dynamics from the Capital University of Science and Technology, Islamabad, Pakistan in 2019. His research interests include nanofluids, heat and mass transfer, magnetohydrodynamics, boundary layer flows, slip flows, and non-linear analysis. He is a reviewer of many international SCI and Scopus journals.

Abid Kamran completed his PhD in July 2020 from Capital University of Science and Technology, Islamabad in the field of Computational Fluid Dynamics. Dr. Kamran has published more than 15 research articles in reputed international journals. He has gained his professional experience spanning over a period of 10 years by serving for many commendable national universities like NUST, CUST, ARID agriculture, and Federal Urdu University, Islamabad. Besides his interest in computational fluid dynamics, his future plans are to explore the field of finance by working on numerical aspects of financial mathematics.